A Low-Inductance Line-Frequency Commutated Rectifier Complying With EN 61000-3-2 Standards

José Antenor Pomilio, *Member, IEEE,* and Giorgio Spiazzi, *Member, IEEE*

***Abstract*—This paper presents a high power factor rectifier, based on a modified conventional rectifier with passive L–C filter, which utilizes a line-frequency-commutated switch and a small auxiliary circuit in order to improve both harmonic content of the input current and power factor, thus allowing compliance with EN 61000-3-2 European standards. Being the switch turned on and off only twice per line period, the associated losses are very small. Moreover the limited di/dt and dv/dt considerably reduce the high-frequency noise emission, thus avoiding heavy EMI filters. The switch operation results in a boost action, which compensates for the filter inductor voltage drop, thus providing output voltage stabilization against load variations. Compared with other similar approaches, the presented topology can achieve higher power levels with a reasonable overall magnetic component size.**

***Index Terms*—Electromagnetic interference, power filters, reactive power, rectifiers.**

I. Introduction

HIGH quality rectifiers (also called power factor correctors—PFCs) are rapidly substituting conventional front-end rectifiers due to harmonic limits imposed by international standards like EN 61000-3-2 [1]. Such high-frequency PFCs provide very high power factors, many times much more than required by the standards and a good output voltage regulation, at the expense of an increase of the overall ac-to-dc converter size and cost. For these reasons, some large volume applications still use standard low cost–high reliable rectifiers with passive filters in order to improve the quality of the current drawn from the line, even if the volume of the reactive components needed becomes rapidly prohibitive as the power increases [2].

Performance improvements of rectifiers with passive filters were achieved in [3] and [4] by adding another capacitor inside the rectifier or even another diode. However, such solutions are useful for an input power up to 300 W, and, being completely passive, they do not provide output voltage stabilization against load variations.

The active solution presented in [5], [6] is, actually, a boost converter operated at line frequency which provides compliance with the standard as well as some degree of output voltage stabilization. However, as the power increases, the inductor value needed makes the solution progressively less interesting. In [7], a modified line-frequency commutated boost rectifier was presented which employs a small line-frequency transformer which allows control of the input current slope at switch turn on, with a consequent reduction of high frequency current harmonics as compared to the simple boost rectifier [5], [6]. A smoother input current waveform, which means compliance with the standard at a reduced input inductor value, was achieved in [8] where a bi-directional low-frequency commutated switch was employed. A noticeable advantage of such solution is the possibility to be used in existing rectifiers with passive L–C filters without interruption of the power flow.

Low-frequency commutation rectifiers have already found application in air conditioning equipment, as presented in [9].

This paper presents another double-line-frequency commutated high-power factor rectifier capable of maintaining EN 61000-3-2 compliance even at high power levels with smaller or comparable overall magnetic components as compared to previous solutions, and, at the same time, it provides output voltage stabilization against load variations. Moreover, the low switching frequency allows reduction of switching losses and EMI filter requirements.

The proposed solution is described in detail in the paper and suitable design criteria are given. Comparison with existing line-frequency commutated rectifiers as well as with standard rectifiers with a passive L–C filter is given, in order to fully highlight advantages and limitation of the proposed solution.

II. Converter Description and Operation

Fig. 1 shows the scheme of the proposed high quality rectifier. Basically, it consists of a standard rectifier with an L–C filter, plus an additional switching unit consisting of two diodes, one switch, one capacitor and one inductor which are all rated at a fraction of the total power delivered to the load. The converter behavior can be better understood with the help of Fig. 2 which reports the simulated circuit main waveforms: auxiliary capacitor voltage u_{Ca}, output voltage U_o, rectified input current i_g, and auxiliary inductor current i_{La}.

The analysis can be broken into two parts: the discharging interval $T_{on}+T_{off}$, at the end of which the auxiliary capacitor C_a is charged at the voltage U_1, and the resonance interval T_1+T_2, in which we have the input current evolution. The switch gate signal can be applied at any instant around the line voltage zero crossing, and it is maintained for an interval T_{on} commanded by the output voltage regulator. During the on interval, which is relatively short compared to the line half-period, capacitor C_a, initially charged at the output voltage U_o, is partially discharged through L_a. Being the voltage across C_a still higher than the input voltage, during this interval, and the subsequent

Manuscript received May 3, 1999; revised May 28, 2002. This work was supported by the Fundação de Amparo à Pesquisa do Estado de São Paulo. Recommended by Associate Editor T. Sloane.

J. A. Pomilip is with the School of Electrical and Computer Engineering, University of Campinas, Campinas 13081-970, Brazil.

G. Spiazzi is with the Department of Electronics and Informatics, University of Padova, Padova 35131, Italy.

Digital Object Identifier 10.1109/TPEL.2002.805597

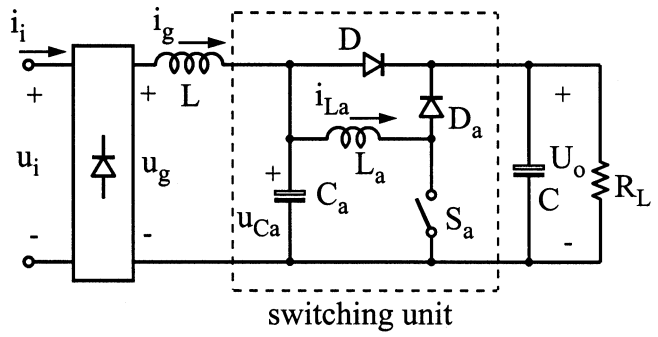

Fig. 1. Scheme of the line frequency commutated rectifier.

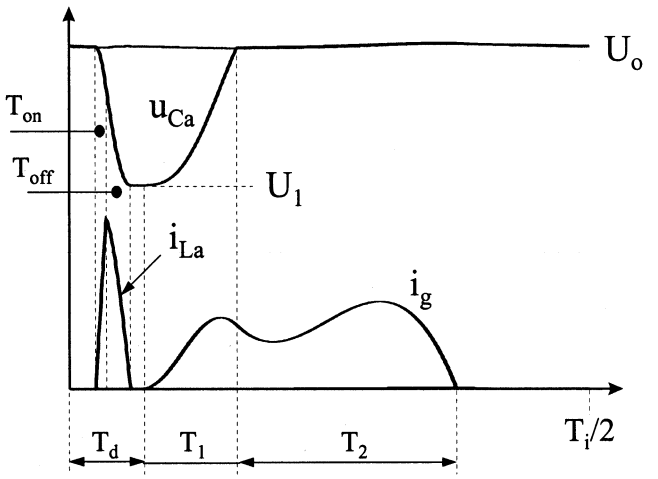

Fig. 2. Rectifier main waveforms: auxiliary capacitor voltage u_{Ca}, output voltage U_o, rectified input current i_g and auxiliary inductor current i_{La}.

one (T_{off}), the input current remains zero. When the switch is turned-off, the current i_{La} flows to the output through diode D_a, continuing to discharge the auxiliary capacitor, until it becomes zero (interval T_{off}). The input current will start to flow at instant T_d when the input voltage becomes equal to the voltage U_1. This occurs earlier respect to the bridge diodes turn-on natural instant due to the lower voltage U_1 as compared to U_o. During this phase, the input inductor resonates with the auxiliary capacitor, giving rise to the smoothed current waveform shown in Fig. 2. When, after interval T_1, voltage u_{Ca} reaches the output voltage value, diode D starts to conduct and now the input inductor resonates with $C + C_a$. In this sense, the auxiliary capacitor can be considered part of the output voltage filter. This phase (interval T_2) lasts until the input current zeros

A detailed description of the converter waveforms is reported in the appendix. Here we want just summarize some results:

• the voltage U_1 across capacitor C_a at the end of the discharge interval as well as the auxiliary switch and diode current stress depend only on the auxiliary inductor and capacitor values and on the switch on-time T_{on}, i.e.:

$$U_1 = U_o\left(1 - \sqrt{2(1-\cos(\omega_a T_{on}))}\right) \tag{1}$$

$$\hat{i}_{La} = \hat{i}_{Sa} = \hat{i}_{Da} = \frac{U_o}{Z_a}\sin(\omega_a T_{on}) \tag{2}$$

where

$$\omega_a = \frac{1}{\sqrt{L_a C_a}} \quad \text{and} \quad Z_a = \sqrt{\frac{L_a}{C_a}}.$$

• similarly to the line frequency boost rectifier presented in [5], [6], the switch voltage stress is simply given by the output voltage U_o.

• the input current waveform depends, besides on the input inductor value, on the resonant frequency $\omega_r = 1/\sqrt{LC_a}$ and on the voltage U_1 across capacitor C_a at the end of the discharge interval. The effects of the different parameters on the input current waveform are analyzed in successive sections.

III. Comparison With Previous Solutions

Many different solutions, based on modified L–C diode rectifier, have already been presented in the literature [3]–[8] aimed to achieve compliance with the EN 61000-3-2 standard. Before the recent modifications of the standard [10], these solutions exploited the difference between the absolute harmonic limits applied to Class A loads and the relative limits applied to Class D loads, for applications below 600 W. Thus, the goal of these modified rectifiers was to change the shape of the input current so as to stay outside the Class D template [1] for at least 5% of the line half period. With the recent modifications introduced into the standard, this trick cannot be used anymore, so that the goal becomes simply to improve the input current harmonic content, irrespective of the power level. In particular, since for the standard passive L–C filter the third harmonic is responsible for the loss of compliance [2], [6], reduction of this harmonic is achieved at the expense of an increase of the high order harmonics. Thus, the latters now set the power limit for such solutions: as an example, Fig. 3 reports the comparison between the passive L–C rectifier and the line frequency commutated boost rectifier of [5], [6] in terms of input current waveform and its spectrum ($U_i = 230\ V_{rms}$, $P_o = 900$ W, $L = 10$ mH). As we can see, the active solution reduces the third harmonic at the expense of an increase of the high order harmonics.

For high power applications, we need solutions able to reduce the third harmonic without excessively increase the high order harmonics, like the converter presented in [8] and the solution proposed here, which provides a smoother input current waveform (see Fig. 2) as compared to that of Fig. 3 (active circuit). However, a meaningful comparison must be done taking into account all the aspects and in particular the higher circuit complexity and the need for a second inductor. To this purpose, the data collected in Table I should help the reader in making this comparison and in selecting the power range in which this rectifier achieves the maximum advantage as compared with other solutions.

The table reports the simulation results of the passive L–C rectifier (P), the proposed active rectifier (A_1) and the boost rectifier (A_2) for three different power levels ranging from 600 up to 1200 W ($U_i = 230\ V_{rms}$). For each power value the following data were collected: average output voltage U_o, inductor current values ensuring compliance with the standard, peak and RMS inductor currents, coefficient $K_L = L \cdot I_{rms} \cdot I_{pk}$, distortion factor $DF = I_{g1rms}/I_{grms}$, displacement factor $\cos(\phi_1)$

TABLE I
COMPARISON AMONG PASSIVE AND ACTIVE RECTIFIERS AT DIFFERENT POWER LEVELS. [P = PASSIVE; A_1 = ACTIVE PROPOSED SOLUTION; A_2 = ACTIVE BOOST RECTIFIER; DF = DISTORTION FACTOR; $\cos(\phi_1)$ = DISPLACEMENT FACTOR; PF = POWER FACTOR]

P_o [W]	U_o [V]	L [mH]	L_a [mH]	I_{gpeak} [A]	I_{grms} [A]	I_{Lapeak} [A]	I_{Larms} [A]	E_L [mJ]	K_L [mJ]	K_{La} [mJ]	DF	$\cos(\phi_1)$	PF
600 - P	*294*	*7*		*8.5*	*3.66*			*253*	*218*		*0.762*	*0.936*	*0.713*
600 - A_1	*318*	*4*	*1*	*7.84*	*3.42*	*14.1*	*2.01*	*123*	*107*	*28.3*	*0.761*	*0.994*	*0.756*
600 - A_2	*298*	*6*		*8.6*	*3.64*			*222*	*188*		*0.756*	*0.948*	*0.717*
900 - P	*258*	*19*		*9.77*	*5.13*			*908*	*953*		*0.888*	*0.859*	*0.763*
900 - A_1	*310*	*6*	*1*	*9.64*	*4.62*	*19.5*	*2.61*	*279*	*267*	*51*	*0.849*	*0.992*	*0.842*
900 - A_2	287.4	10		9.88	4.82			488	476		0.93	0.859	0.799
1200 - A_1	*300*	*8*	*2*	*10.9*	*5.76*	*20.9*	*3.3*	*475*	*502*	*138*	*0.908*	*0.989*	*0.898*
1200 - A_2	*268*	*18*		*11.19*	*6.22*			*1128*	*1254*		*0.924*	*0.907*	*0.838*

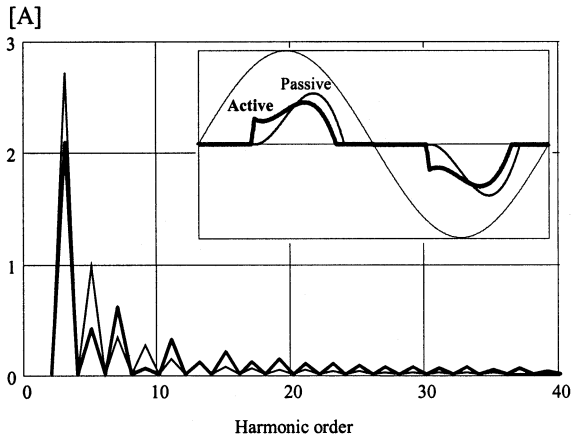

Fig. 3. Current spectrum comparison between the passive L–C rectifier and the line frequency commutated boost converter. ($U_i = 230\ V_{rms}$, $P_o = 900$ W, $L = 10$ mH).

and power factor $PF = DF \cdot \cos(\phi_1)$. Coefficient K_L is related to the core size and is proportional to the product between the iron cross-section A_e and the core window area A_w as it will be shown later. It is also related to the inductor peak energy, i.e., $K_L = 2\,E_L/CF$ where $CF = I_{pk}/I_{rms}$ is the crest factor. These data show that, in this power range, the proposed solution allows a considerable reduction of the total magnetic component size as compared with both the passive filter and the line-frequency-commutated boost. Note, also, the higher output voltage achievable as a consequence of a lower input inductor value and of the switch boost action.

A comparison among some low and high-frequency (HF) commutation PFC's (boost topology) was presented in [11]. For the HF commutation PFC, the converter losses are concentrated in the power switch, what means that the transistor and the fast diode heatsinks are much bigger than in the low-frequency commutation case, in which the losses are concentrated in the inductor. Especially in the kW range, another relevant aspect is the EMI filter size. The volume of a standard EMI filter is comparable to the low-frequency PFC inductor volume. Of course there are some alternatives to reduce the EMI emission, like soft-commutation techniques, that should be considered for a more precise comparison among the resulting power densities. The conclusion is that the power density of a low-frequency PFC can be comparable to the HF solution, if considered the overall converter volume, including heatsinks and EMI filters.

IV. DESIGN CONSIDERATIONS

The choice of the converter parameters depends on the designer objective. In fact, if the goal is just to comply with the standard without looking for a deep output voltage regulation, then the minimum switch on-time should be used, since it strongly affects the auxiliary inductor size and auxiliary switch and diode current stress, as can be seen by (2). On the other hand, allowing higher T_{on} values, an increase in the converter boost action is achieved, thus increasing the output voltage regulation against both line and load variations. In the following the analysis will be limited to the objective of achieving compliance with the standard at the minimum cost, i.e., minimum size and device stresses.

A. Analysis of the Input Current Waveform

The input inductor waveform is influenced by three main factors: input inductor value, auxiliary capacitor value, which sets the resonant frequency during the secondary resonance interval T_1 and residual voltage U_1 on capacitor C_a at the end of the discharging process. Since the effects of these different factors combine together in a way that is very hard to put in correlation with the input current spectrum, simulation must be used in order to verify the design choices. Here, some simulations are reported which help to make a reasonable parameter value first estimation.

The effect of capacitor C_a can be analyzed by looking at Fig. 4: it shows the input current waveform and its spectrum at different values of parameter $\alpha = \omega_r/\omega_i$ at constant output power and normalized voltage $U_{1N} = U_1/U_o$ ($\omega_r = 1/\sqrt{LC_a}$ and ω_i: line voltage angular frequency). As we can see, higher C_a values (lower α) cause lower harmonic amplitudes, except for the third and ninth ones, together with lower peak current values. However, of the three waveforms, that corresponding to $\alpha = 5$ is the only which does not comply with the standard. Moreover, high C_a values cause high switch current stress since, at constant U_{1N} values, the current stress is proportional to the square root of C_a [from (1) and (2)].

As far as the effect of voltage U_1 is concerned, Fig. 5 shows the simulation results at different U_{1N} values at constant output power and converter parameters values. Actually, changing of voltage U_1 is achieved modifying the switch on-time. Decreasing U_1 causes a reduction of dead time T_d as well as reduction of third, ninth and thirteenth harmonics, while other

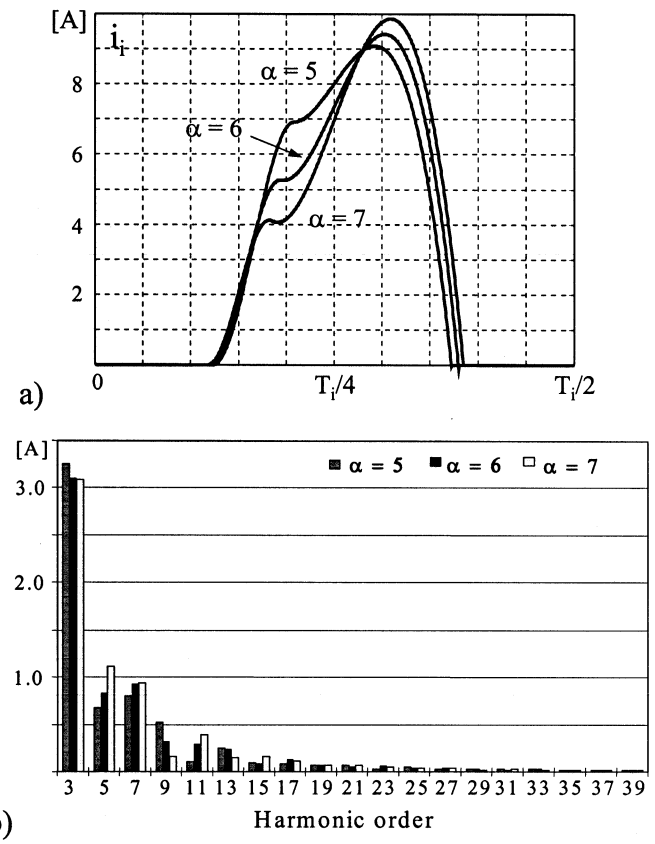

Fig. 4. Effect of variation of capacitor $C_a(\alpha = \omega_r/\omega_i)$. (a) Input current waveforms; (b) input current spectrum (peak value) ($U_i = 230\ V_{rms}$, $P_o = 900$ W, $L = 6$ mH, $L_a = 1$ mH, $U_{1N} = 0.72$).

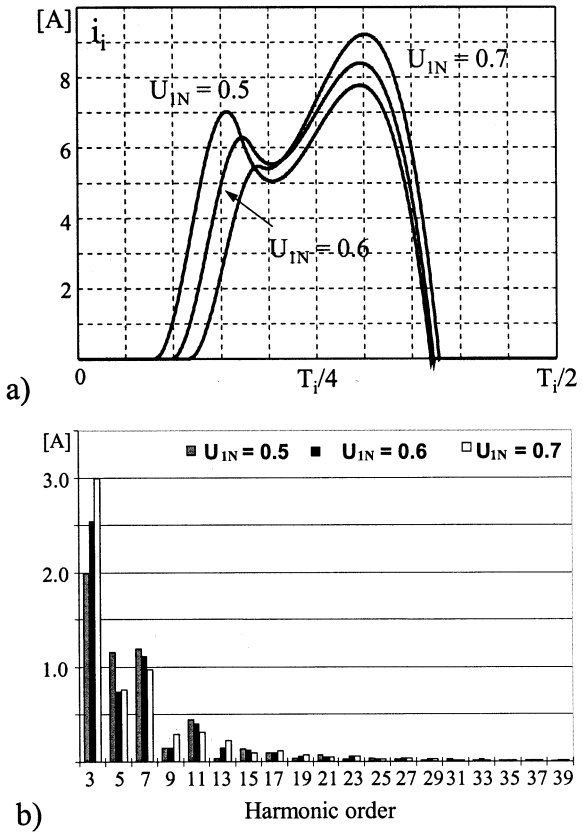

Fig. 5. Effect of variation of voltage U_1 ($U_{1N} = U_1/U_o$). (a) Input current waveforms; (b) input current spectrum (peak value) ($U_i = 230\ V_{rms}$, $P_o = 900$ W, $L = 6$ mH, $L_a = 1$ mH, $\alpha = 6$).

harmonics increase. The peak input current is also decreased. However, only the waveform corresponding to $U_{1N} = 0.7$ complies with the standard. Moreover, lower U_1 values mean higher T_{on} value and consequently increase of the switch current stress.

From both Figs. 4 and 5, we can see that the purpose of the switching unit should be to modify as little as possible the input current waveform as compared to that of the standard *L–C* rectifier, thus causing a decrease of the third harmonic amplitude below the limit without excessive increase of the high order harmonic amplitudes and with the minimum switching unit size.

B. Selection of L_a

The objective of this work is to provide compliance with the standards with a reduced overall magnetic component size as compared to previous solutions. To this purpose, the switch on-time should be kept as small as possible since it strongly affect the auxiliary inductor size and auxiliary switch and diode current stress, as can be seen by (2). Minimization of the auxiliary inductor size is accomplished by choosing the minimum value for inductor L_a taking into account the allowed switch current stress. In fact, the inductor core volume is related to the product between the iron cross-section A_e and the core window area A_w, i.e.:

$$A_w A_e = \left(\frac{N}{k_R}\frac{I_{Larms}}{J}\right)\left(\frac{L_a I_{Lapk}}{N B_{\max}}\right) = \frac{K_{La}}{k_R J B_{\max}} \quad (3)$$

where $B_{\max}$ is the maximum flux density, J is the desired current density and k_R the window filling coefficient.

A plot of coefficient K_{La} as a function of inductor value L_a is reported in Fig. 6 for three different value of voltage U_1 showing a monotonic increase with the inductor value and a strong dependence on voltage U_1, as already stated above.

C. Selection of Output Capacitor C

For the selection of the output capacitor value, a good guess is the value obtained by the approximate analysis of the classical diode-bridge with capacitive filter rectifier, i.e.:

$$C = \frac{\pi P_o}{\omega_i U_o \Delta U_o} \quad (4)$$

where ΔU_o is the maximum allowed output voltage ripple (peak-to-peak). Note that due to the switching unit operation, the effective output voltage ripple will be lower than ΔU_o because of the extended diode bridge conduction angle as well as because of the energy delivered by the auxiliary inductor to the output capacitor in a moment in which it would be discharging in the conventional rectifier.

D. Design Example

In order to give an idea of the magnetic component size, let us consider a practical example:

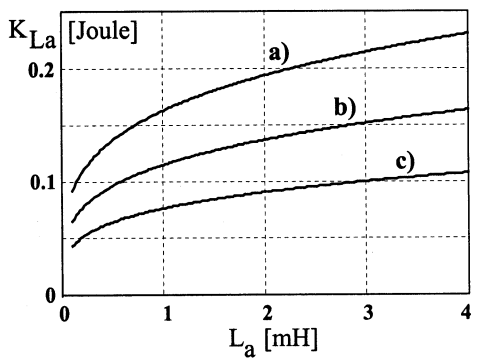

Fig. 6. Coefficient K_{La} as a function of the auxiliary inductor value. (a) $U_{1N} = 0.4$; (b) $U_{1N} = 0.5$; (c) $U_{1N} = 0.6$. ($U_i = 230\ V_{rms}$, $P_o = 900$ W).

Converter specifications:

$$U_i = 220\,V_{rms} \pm 20\%, \quad P_o = 900\ \text{W}, \quad L = 6\ \text{mH},$$
$$L_a = 1\ \text{mH}, \quad C_a = 44\ \mu\text{F}, \quad T_{on} = 60\ \mu\text{s}.$$

The material used for both the main and auxiliary inductors has the following parameter values:

$$\textit{relative permeability}: \quad \mu_r = 11\,674$$
$$\textit{flux density}: \quad B = 1.35\ \text{T}.$$

The utilized window filling coefficient k_R is 0.4, and the current density J is 3 A/mm^2. The auxiliar inductor parameters are:

$$\textit{iron cross section}: \quad A_e = 1.6 \cdot 10^{-4}\ \text{m}^2$$
$$\textit{number of turns}: \quad N_a = 85$$
$$\textit{wire diameter}: \quad \Phi_a = 1\ \text{mm}$$
$$\textit{external core volume}: \quad Vol = 1.96 \cdot 10^{-5}\ \text{m}^3.$$

The main inductor parameters, calculated for the maximum input current (i.e., minimum input voltage), are:

$$\textit{iron cross section}: \quad A_e = 7.7 \cdot 10^{-4}\ \text{m}^2$$
$$\textit{number of turns}: \quad N = 69$$
$$\textit{air gap}: \quad t_{gap} = 0.38\ \text{mm}$$
$$\textit{wire diameter}: \quad \Phi = 1.6\ \text{mm}$$
$$\textit{external core volume}: \quad Vol = 1.27 \cdot 10^{-4}\ \text{m}^3.$$

The rectifier output voltage at the minimum input voltage and nominal power is 227 V.

For the sake of comparison a similar design was carried out for the passive solution. The inductor value needed to comply with the standard for the same converter specification is 19 mH. The resulting inductor parameters are:

$$\textit{iron cross section}: \quad A_e = 1.28 \cdot 10^{-3}\ \text{m}^2$$
$$\textit{number of turns}: \quad N = 131$$
$$\textit{air gap}: \quad t_{gap} = 0.73\ \text{mm}$$
$$\textit{wire diameter}: \quad \Phi = 1.7\ \text{mm}$$
$$\textit{external core volume}: \quad Vol = 3.24 \cdot 10^{-4}\ \text{m}^3.$$

The rectifier output voltage at the minimum input voltage and nominal power is 179 V.

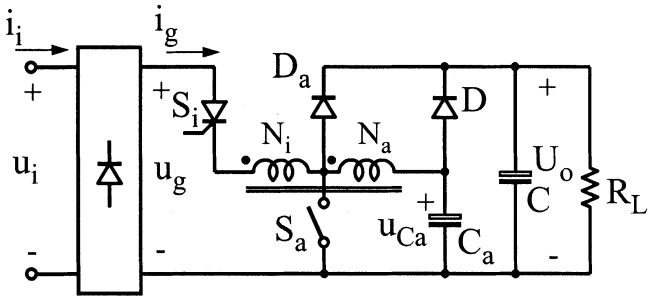

Fig. 7. Modified rectifier scheme with coupled inductors.

E. Output Voltage Regulation

As far as the output voltage regulation is concerned, we must consider separately the effects of load and input voltage variations, having in mind the constraint imposed by the maximum switch on-time that strongly affect the switching unit size. Thus, once we have selected the maximum T_{on} in order to accomplish compliance with the standards at nominal load and prescribed input voltage, the control can only reduce the switch on-time at load current decreasing. A standard PI regulator having a bandwidth well below the line frequency, like any other PFC regulator, is sufficient to accomplish this. Clearly, a minimum power level exists below which the output voltage regulation cannot be maintained, and it corresponds to the value for which the passive L–C rectifier (without the switching unit) achieves the same output voltage. At lower power levels, the output voltage increases toward the input voltage peak, like any standard rectifier. For this reason, a high output voltage reference is preferable, since it can be maintained for a broader load variation.

As far as the line voltage variation is concerned, having imposed a maximum switch on-time, the regulation of the output voltage can be maintained only for a small input voltage increase (which requires reduction of the switch on-time), while, at low input voltage, T_{on} is kept constant and equal to the maximum value allowed by the switching unit design, causing the decrease of the output voltage too.

V. Topology Variation

The circuit discussed so far has the disadvantage to use two separate inductors, thus it is worthy to study the possibility of using only one magnetic core. A scheme that basically works as the previous one but employs only one tapped inductor is shown in Fig. 7. Differently from the previous one, this circuit contains one more line-frequency commutated switch S_i which can be implemented using a SCR. For a better understanding of its operation principle let us assume the switch S_i is off at the beginning of the line half period. The capacitor discharge phase occurs through winding N_a when switch S_a is turned on and it continues through diode D_a during T_{off}, causing voltage u_{Ca} to drop at U_1 level (see Fig. 2). Switch S_i prevents conduction of the bridge diodes during the T_{on} interval since voltage u_{Ca} reflects in the N_i winding with the right polarity to cause a premature bridge diode turn on. When S_i is turned on the resonant interval starts involving the overall inductance (corresponding

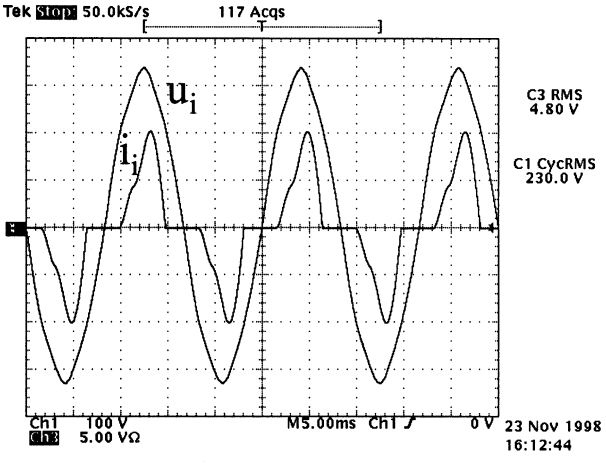

Fig. 8. Measured Input voltage u_i (100 V/div) and input current i_i (5 A/div) of the proposed rectifier of Fig. 1 ($U_i = 230\ V_{rms}$, $P_o = 900$ W).

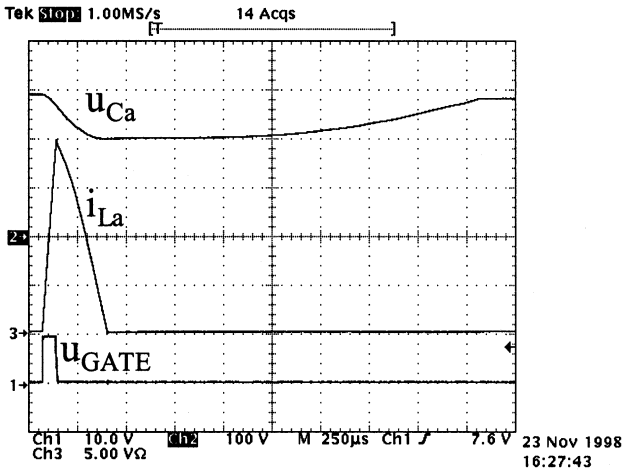

Fig. 9. Measured auxiliary capacitor voltage u_{Ca} (100 V/div), auxiliary inductor current i_{La} (5 A/div) and switch gate drive signal U_{GATE} (10 V/div) of the proposed rectifier of Fig. 1 ($U_i = 230\ V_{rms}$, $P_o = 900$ W).

to $N_i + N_a$) and the input current evolution is similar to what we have already shown in Fig. 2. However, coupling the two inductors imposes a constraint on the circuit that is in order to have a behavior similar to that of the original rectifier, diode D_a must remain off during interval $T_1 + T_2$. This condition is satisfied if the output voltage is greater than the peak input voltage. In fact, the diode voltage during this interval is given by:

$$U_{Da} = u_{Ca} + \frac{u_g - u_{Ca}}{1+n} - U_o.$$

For U_{Da} to be negative must be $n > (u_g - U_o)/(U_o - u_{Ca})$ which is satisfied only if $U_o > U_{gpk}$, since the denominator tends to zero (see Fig. 2). For such circuit, the inductor coefficient K_L, which can be used as an estimation of the magnetic component volume, is given by the following expression:

$$K_L = \frac{L}{1+n} \cdot \max\left\{\frac{I_{Lapk}}{1+n}, I_{gpk}\right\} \cdot \left(nI_{grms} + \sqrt{I_{grms}^2 + I_{Larms}^2}\right) \quad (5)$$

where $n = N_i/N_a$, and i_{La} denotes the current in winding N_a during the discharge phase. This expression takes into account the possibility that the maximum flux in the core occurs during the discharge phase (in winding N_a) instead of during the resonant phase (in winding $N_i + N_a$).

In order to compare this topology variation with the original rectifier we can make the following considerations:

- the need for an output voltage higher than the input voltage requires higher T_{on} values as compared to the original circuit, in order to increase the converter boost action. As a consequence, a global filter inductor value very close to the sum of the two separated inductor values employed in Fig. 1 is required in order to meet the standards;
- the high peak current during the discharge phase, consequence of an increased T_{on}, causes a higher inductor coefficient K_L as compared to the original circuit. However, since the maximum flux in the core usually occurs during the discharge phase [see eq. (5)], it remains unchanged at lower input voltages (actually it decreases due to the lower output voltage value), while for the original rectifier the maximum flux in the input inductor increases due to the higher input current peak;
- the high output voltage gives to the circuit the capability of maintaining a fairly regulated output voltage in a greater load range as compared to the original one. Actually, being $U_o > U_{ipk}$, the output voltage can be maintained down to no load by simply reducing the on time of switch S_a.

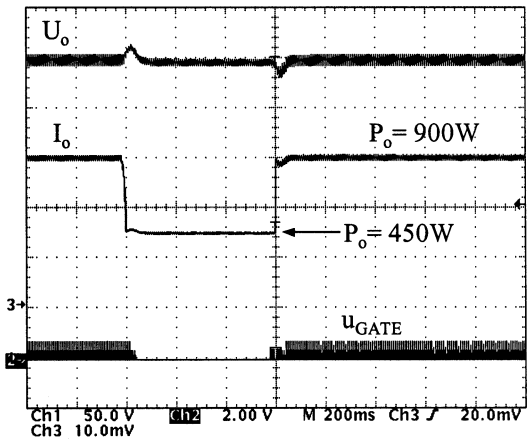

Fig. 10. Load variation dynamic response ($U_i = 230\ V_{rms}$, 450 W to 900 W): output voltage U_o (top trace—50 V/div), load current I_o (center trace—1 A/div) and switch command U_{GATE} (bottom trace—20 V/div).

VI. Experimental Measurements

In order to verify the results obtained by simulation a prototype of the circuit shown in Fig. 1 was built having the following specifications: $U_i = 230\,V_{rms}$, $U_o = 292$ V, $P_o = 900$ W, $f_i = 60$ Hz, $L = 6$ mH, $L_a = 1$ mH, $C_a = 44$ μF, $C = 1200$ μF.

The rectifier input current and voltage waveforms at nominal conditions are shown in Fig. 8 and the corresponding current harmonics amplitudes are reported in Table II, together with Class A limits. As can be seen, the input current waveform well

TABLE II
MEASURED INPUT CURRENT HARMONICS FOR THE PROPOSED RECTIFIER

I_n	Harm. [A_{rms}]	Class A limits [A_{rms}]
I_3	2.18	2.30
I_5	0.73	1.14
I_7	0.46	0.77
I_9	0.028	0.40
I_{11}	0.14	0.33
I_{13}	0.05	0.21
I_{15}	0.058	0.15
I_{17}	0.048	0.132
I_{19}	0.022	0.118
I_{21}	0.026	0.107

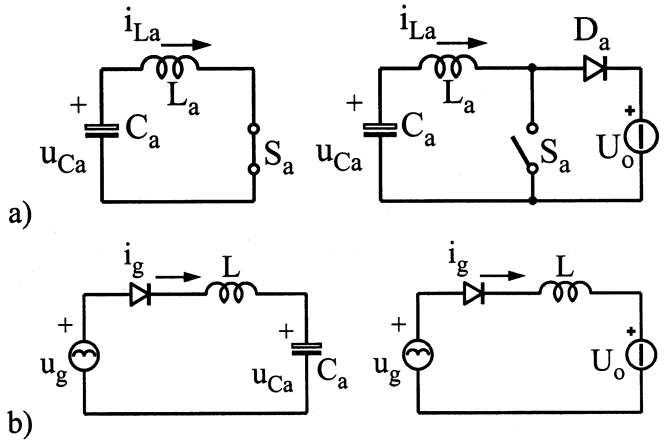

Fig. 11. Converter sub-topologies in a line half period. (a) Discharge interval $T_{on} + T_{off}$; (b) resonance interval $T_1 + T_2$.

agrees with the simulation results and all the harmonics are well below their limits. The employed switch on-time is 70 μs, as we can see from Fig. 9 which reports the auxiliary capacitor voltage u_{Ca}, the auxiliary inductor current i_{La} and the switch gate drive signal at the beginning of the line half period. Comparing such waveforms with the idealized ones of Fig. 2 allows easily recognition of subintervals T_{on}, T_{off}, T_d and T_1. The switch current stress is about 20 A, while the output voltage limits its voltage stress. The measured efficiency is 96%, not including control and driving losses, while the power factor is 0.85, and it is almost totally dominated by the distortion factor DF which results 0.86 (THD $= 59\%$).

Fig. 10 shows the dynamic response to a load variation between 450 and 900 W. The control loop uses a PI controller. As can be seen the control system is able to maintain the output voltage regulation. Bellow 450 W, as the auxiliary switch does not conduct anymore and the voltage output increases up to reach the input voltage peak value (325 V). For the input voltage variation, the system is able to regulate the output up to a 5% over-voltage (241 V).

VII. CONCLUSION

The paper has presented a modification of conventional rectifiers with a passive L–C filter that helps to make compliance with harmonic standard with a reduced overall magnetic component size as compared to previous solutions. The added switching unit employs a line frequency commutated switch rated at a fraction of the total power delivered to the load. Its inherent boost action allows regulation of the output voltage against load variations, without affecting the converter efficiency. A topology modification employing only one magnetic core was also presented and its performances discussed in comparison with the original circuit.

Measurements on a 900 W prototype have shown a good agreement with theoretical expectations.

APPENDIX

In order to derive the input current equations during the different time intervals in the line half period let us refer to Fig. 2 waveforms and to Fig. 11 that reports the converter sub-topologies. The following equations hold on the assumption that during the total discharge interval of capacitor C_a ($T_{on} + T_{off}$) the input current stays at zero since the rectified input voltage is lower than u_{Ca}. Moreover the output capacitor is considered big enough to maintain constant the output voltage. The rectified input voltage is $u_g(t) = \hat{U}_g\,|\sin(\omega_i t)|$.

1) Discharge interval

a) $0 \le t \le T_{on}$. A resonance between C_a and L_a occurs $\left(\omega_a = \dfrac{1}{\sqrt{L_a C_a}}\; Z_a = \sqrt{\dfrac{L_a}{C_a}}\right)$:

$$\begin{aligned} i_{La}(t) &= \frac{U_o}{Z_a}\sin(\omega_a t) \\ u_{Ca}(t) &= U_o\cos(\omega_a t). \end{aligned} \tag{A.1}$$

b) $T_{on} \le t \le T_{on} + T_{off}$. C_a continues discharging until current i_{La} zeros

$$\begin{aligned} i_{La}(t) &= I_{a0}\cos(\omega_a(t - T_{on})) - \frac{U_o - U_{a0}}{Z_a}\sin(\omega_a(t - T_{on})) \\ u_{Ca}(t) &= U_o - Z_a I_{a0}\sin(\omega_a(t - T_{on})) \\ &\quad - (U_o - U_{a0})\cos(\omega_a(t - T_{on})) \end{aligned} \tag{A.2}$$

where the initial conditions I_{a0} and U_{a0} are given by:

$$\begin{aligned} I_{a0} &= \frac{U_o}{Z_a}\sin(\omega_a T_{on}) \\ U_{a0} &= U_o\cos(\omega_a T_{on}). \end{aligned} \tag{A.3}$$

Interval T_{off} can be calculated setting current i_{La} to zero, i.e.:

$$T_{off} = \frac{1}{\omega_a}\,a\tan\left(\frac{\sin(\omega_a T_{on})}{1 - \cos(\omega_a T_{on})}\right). \tag{A.4}$$

The voltage across C_a at the end of the discharge interval $T_{on} + T_{off}$ is given by:

$$U_1 = U_o\left(1 - \sqrt{2\,(1 - \cos(\omega_a T_{on}))}\right). \tag{A.5}$$

2) Secondary resonance interval $T_d \le t \le T_d + T_1$.

This interval starts at $t = T_d$ when the rectified input voltage becomes equal to voltage U_1 across C_a, i.e.,

$$T_d = \frac{1}{\omega_i}\, a\sin\left(\frac{U_1}{\hat{U}_g}\right) \tag{A.6}$$

$$a_i = -b_i\sqrt{\left(\frac{\hat{U}_g}{U_1}\right)^2 - 1} \quad a_u = -b_u\sqrt{\left(\frac{\hat{U}_g}{U_1}\right)^2 - 1}$$

$$b_i = -\frac{U_1}{\omega_i L}\left(\frac{1}{\alpha^2 - 1}\right) \quad b_u = -U_1\left(\frac{\alpha^2}{\alpha^2 - 1}\right) \tag{A.7a}$$

$$i_g(t) = a_i\left[\cos(\omega_i(t - T_d)) - \cos(\omega_r(t - T_d))\right] + b_i\left[\sin(\omega_i(t - T_d)) - \frac{1}{\alpha}\sin(\omega_r(t - T_d))\right] \tag{A.7b}$$

$$u_{Ca}(t) = U_1 + a_u\left[\sin(\omega_i(t - T_d)) - \frac{1}{\alpha}\sin(\omega_r(t - T_d))\right] + b_u\left[(1 - \cos(\omega_i(t - T_d))) - \frac{1}{\alpha^2}(1 - \cos(\omega_r(t - T_d)))\right] \tag{A.7c}$$

where $\omega_r = 1/\sqrt{L\,C_a}$ and $\alpha = \omega_r/\omega_i$. This interval ends when the voltage across the auxiliary capacitor C_a reaches the output voltage value, i.e., $u_{Ca}(T_d + T_1) = U_o$. Let us indicate the input current value at this instant as I_{g0}.

3) Main resonance interval $T_d + T_1 \le t \le T_d + T_1 + T_2$

$$i_g(t) = I_{g0} + \frac{\hat{U}_g}{\omega_i L}\left[\cos(\omega_i(T_d + T_1)) - \cos(\omega_i t) - \frac{U_o}{\hat{U}_g}\,\omega_i(t - T_d - T_1)\right]. \tag{A.8}$$

After interval T_2, the input current zeros and remains zero until the next line half period.

ACKNOWLEDGMENT

The authors would like to thank E. da Silva Martins for the prototype implementation and testing.

REFERENCES

[1] EN61000-3-2, "Limits for harmonic current emissions (equipment input current up to and including 16A per phase)," European Committee for Electrotechnical Standardization, Belgium, Mar. 1995.

[2] M. Jovanovic and D. E. Crow, "Merits and limitations of full-bridge rectifier with LC filter in meeting IEC 1000-3-2 harmonic-limit specifications," in *Proc. IEEE Appl. Power Electron. Conf. (APEC)*, Mar. 1996, pp. 354–360.

[3] R. Redl and L. Balogh, "Power-factor correction in bridge and voltage-doubler rectifier circuits with inductors and capacitors," in *Proc. IEEE Appl. Power Electron. Conf. (APEC)*, Mar. 1995, pp. 466–472.

[4] R. Redl, "An economical single-phase passive power-factor-corrected rectifier: Topology, operation, extensions, and design for compliance," in *Proc. IEEE Appl. Power Electron. Conf. (APEC)*, Feb. 1998, pp. 454–460.

[5] I. Suga, M. Kimata, Y. Ohnishi, and R. Uchida, "New switching method for single-phase AC to DC converter," in *Proc. Power Conv. Conf.*, Tokyo, Japan, 1993, pp. 93–98.

[6] L. Rossetto, G. Spiazzi, and P. Tenti, "Boost PFC with 100Hz switching frequency providing output voltage stabilization and compliance with EMC standards," *IEEE Trans. Ind. Applicat.*, vol. 36, pp. 188–193, Jan./Feb. 2000.

[7] G. Spiazzi and S. Buso, "A line-frequency commutated rectifier complying with IEC 1000-3-2 standard," *IEEE Trans. Ind. Electron.*, vol. 47, pp. 501–510, June 2000.

[8] G. Spiazzi, E. da Silva Martins, and J. A. Pomilio, "A simple line-frequency commutation cell improving power factor and voltage regulation of rectifiers with passive L–C filter," in *Proc. IEEE Power Electron. Spec. Conf. (PESC)*, June 2001, pp. 724–729.

[9] Y. Shimma and K. Iida, "Inverter applications to air conditioning field," in *Proc. Int. Power Electron. Conf. (IPEC'00)*, Japan, May 2000, pp. 1747–1750.

[10] Amendment A14 to EN61000-3-2, "Limits for harmonic current emissions (equipment input current up to and including 16A per phase)," European Committee for Electrotechnical Standardization, Belgium, Mar. 2000.

[11] J. A. Pomilio, G. Spiazzi, and S. Buso, "Comparison among high-frequency and line-frequency commutated rectifiers complying with IEC 61 000-3-2 standards," in *Proc. IEEE Ind. Applicat. Soc. Annu. Meeting—IAS'00*, Oct. 2000.

José Antenor Pomilio (M'02) was born in Jundiaí, Brazil, in 1960. He received the B.Sc., M.Sc., and D.Sc. degrees in electrical engineering from the University of Campinas (UNICAMP), Campinas, Brazil, in 1983, 1986, and 1991, respectively.

From 1988 to 1991, he was head of the Power Electronics Group, Brazilian Synchrotron Laboratory. Since 1991, he has been an Assistant Professor at the School of Electrical and Computer Engineering, University of Campinas. From 1993 to 1944, he held a post-doctoral position at the Electrical Engineering Department, University of Padova, Italy. He currently is President of the Brazilian Power Electronics Society and at-large member of the IEEE Power Electronics Society Administrative Committee. His main interests are switching mode power supplies, electrical drives, and active power filters.

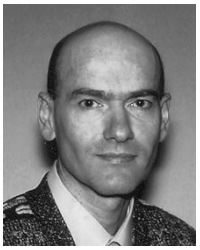

Giorgio Spiazzi (S'92–M'95) was born in Verona, Italy, in 1962. He received the M.S. degree (with honors) and the Ph.D. degree in industrial electronics and informatics from the University of Padova, Padova, Italy, in 1988 and 1993, respectively.

He was a Researcher in the Department of Electronics and Informatics, University of Padova. In 2001, he became Assistant Professor in the same university. His main research interests are in the fields of advanced control techniques of dc/dc converters, high power factor rectifiers, soft-switching techniques, and electromagnetic compatibility in power electronics.